Biosensors and Bioelectronics 24 (2008) 696–703

Contents lists available at ScienceDirect

Biosensors and Bioelectronics

journal homepage: www.elsevier.com/locate/bios

# Microscopic mechanisms influencing the volume amplified magnetic nanobead detection assay

M. Strömberg[a], T. Zardán Gómez de la Torre[a], J. Göransson[b], K. Gunnarsson[c], M. Nilsson[b,*], M. Strømme[a,*], P. Svedlindh[c,*]

[a] Department of Engineering Sciences, Division of Nanotechnology and Functional Materials, Uppsala University, The Ångström Laboratory, Box 534, SE-751 21 Uppsala, Sweden
[b] Department of Genetics and Pathology, Uppsala University, Rudbeck Laboratory, SE-751 85 Uppsala, Sweden
[c] Department of Engineering Sciences, Division of Solid State Physics, Uppsala University, The Ångström Laboratory, Box 534, SE-751 21 Uppsala, Sweden

ARTICLE INFO

*Article history:*
Received 28 March 2008
Received in revised form 19 June 2008
Accepted 23 June 2008
Available online 6 July 2008

*Keywords:*
Bioassay development
Brownian relaxation
Padlock probes
Rolling circle amplification
Probe-tagged magnetic beads
Microscopic mechanisms

ABSTRACT

The volume amplified magnetic nanobead detection assay [Strömberg, M., Göransson, J., Gunnarsson, K., Nilsson, M., Svedlindh, P., Strømme, M., 2008. Nano Letters 8, 816–821] was investigated with respect to bead size, bead surface coverage of probe oligonucleotides, bead concentration and rolling circle amplification (RCA) time, with the objective to improve the understanding of the microscopic mechanisms influencing the assay. The most important findings for future biosensor development were the following: (i) small beads exhibit a much reduced tendency to cross-link several RCA products, thus enabling use of both complex magnetisation *turn-on* and *turn-off detection* strategies, whereas larger beads only allow for *turn-off* detection; (ii) small beads exhibit faster *immobilisation kinetics*, thus reducing the time for diagnostic test completion, and also immobilise in larger numbers than larger beads. Finally, (iii) by demonstrating qualitative dual-target detection of bacterial DNA sequences using 130 and 250 nm beads, the bioassay was shown to allow for *multiplexed detection*.



## 1. Introduction

Today, magnetic nanoparticles, commonly referred to as magnetic beads, are used in many research and technology areas including biotechnology, biomedicine and drug discovery (Saiyed et al., 2003). Biofunctionalised magnetite beads find, due to their magnetic properties and biocompatibility, many promising applications in biodiagnostic and therapeutic methodologies such as bioassays and magnetic separation, as contrast agents in magnetic resonance imaging, as well as in drug-delivery and hyperthermia cancer treatment (Salata, 2004; Mornet et al., 2004; Osaka et al., 2006; Liu, 2006; Majewski and Thierry, 2007). Magnetic bead-based bioassays often involve labelling magnetic beads with probe biomolecules and upon interaction with the target, either the static or dynamic magnetic bead properties are detected. Furthermore, magnetic biosensor schemes are either classified as substrate-based (sensor on chip) or substrate-free. In the former biosensor category, if target is present, probe biofunctionalised magnetic beads bind directly to the sensor surface, thereby inducing a signal change. Examples of existing chip-based systems are Hall effect (Sandhu et al., 2007) and magnetoresistive micro-biosensor platforms (Freitas et al., 2007). One substrate-free method is the Brownian relaxation biosensor scheme (Connolly and St Pierre, 2001), which makes use of the decrease in the bead Brownian relaxation frequency caused by the hydrodynamic size increase upon probe–target coupling. This biosensor format has, e.g. been tested in immunoassays (Astalan et al., 2004; Hong et al., 2007). Furthermore, as pointed out in Wang (2005), signal amplification is necessary for achieving ultrasensitive miniaturised bioassays. Moreover, high sensitivity methods are needed for detecting disease diagnosis markers present at very low levels during early stages of disease progress (Wang, 2005). While the polymerase chain reaction has revolutionised genetic testing, it is somewhat restricted owing to its complexity, potential contamination risk and cost. Another, more practically convenient target detection and amplification strategy exhibiting high specificity and selectivity is padlock probe target recognition (Nilsson et al., 1994; Landegren et al., 2003) followed by rolling circle amplification (RCA) (Fire and Xu, 1995; Liu et al., 1996).

Recently, we demonstrated a novel non-fluorescence high sensitivity biomolecule detection method combining padlock probe target recognition and RCA with the Brownian relaxation

* Corresponding authors. Tel.: +46 18 471 0000.
*E-mail addresses:* mats.nilsson@genpat.uu.se (M. Nilsson), maria.stromme@angstrom.uu.se (M. Strømme), peter.svedlindh@angstrom.uu.se (P. Svedlindh).

0956-5663/$ – see front matter © 2008 Elsevier B.V. All rights reserved.
doi:10.1016/j.bios.2008.06.043

biosensor scheme; the volume amplified magnetic nanobead detection assay (Strömberg et al., 2008). A limit of detection (LOD) of 4 pM was achieved and the system was optimised mainly with respect to the sample preparation conditions. Briefly, the assay relies on padlock probe target recognition followed by RCA for a certain time, the RCA-time, giving an ensemble of DNA macromolecules (RCA-coils) (~1 μm size for a RCA-time of 1 h), which in turn are detected by oligonucleotide tagged magnetic nanobeads binding to the RCA-coils by base-pair hybridisation. This causes a dramatic change in the bead Brownian relaxation frequency due to the strongly increased bead hydrodynamic volume, now essentially corresponding to the size of an RCA-coil. We denote this bead binding process *bead immobilisation* since upon binding to RCA-coils, beads are no longer free in solution and their Brownian relaxation is strongly hindered. Upon immobilisation, the magnitude of the imaginary part of the frequency-dependent complex magnetisation ($m = m' - im''$) at the Brownian relaxation frequency ($f_B$) for non-immobilised beads, the $m''$ *high frequency peak* (HFP) level, decreases. Single RCA-coils containing immobilised beads exhibit a relaxation peak, which we denote the *low frequency peak* (LFP). The HFP level was used as read-out principle in (Strömberg et al., 2008).

In the present work, we investigate in more detail how experimental parameters such as bead size, bead concentration, bead surface coverage of probe molecules and RCA-time affect the bioassay system with the objective to further develop the bioassay principle. Central issues in the study are to find out if *other read-out principles* than the turn-off type detection is possible depending on bead size and to evaluate *immobilisation characteristics* for various bead sizes. Finally, *multiplexing possibilities* are evaluated by qualitatively performing dual-target detection of bacterial DNA-sequences.

## 2. Materials and methods

### 2.1. Oligonucleotide detection probe-tagged bead synthesis using SPDP coupling chemistry and analysis of oligonucleotide coupling yield

Three aqueous suspensions of monodisperse amino-functionalised cluster-type magnetic beads (nanomag®-D $NH_2$; Micromod Partikeltechnologie GmbH) having bead diameters of 40, 130 and 250 nm were used in this study. The oligonucleotide surface functionalisation procedure was similar to that presented earlier (Strömberg et al., 2008) but with some modifications as outlined in the supplementary material, section A. Table 1 lists synthesis conditions and properties for the probe-tagged bead batches as well as specifies detection probe sequences for each batch.

### 2.2. Padlock probe target recognition and RCA

The procedures for performing target recognition and RCA were similar to those described in Strömberg et al. (2008) except for using other target and padlock probe sequences (cf. Table 1).

### 2.3. Sample preparation and characterisation

A SQUID magnetometer was used to measure the frequency-dependent complex magnetisation (1000–0.5 Hz) and saturation magnetisation of each sample. In all ac magnetisation measurements, the drive amplitude of the ac field was 2 Oe. In order to obtain the saturation magnetisation of each sample, the diamagnetic contribution from the sample holder was subtracted. The saturation magnetisation was used to calculate the actual amount of beads in a sample.

#### 2.3.1. Characterisation of batches of probe-tagged beads and non-functionalised beads

30 μl of the batch solution of probe-tagged beads or of non-functionalised beads was vortexed during 1 min at room temperature and thereafter mounted in the SQUID for measurements of the complex magnetisation and the saturation magnetisation at 310 K.

#### 2.3.2. Characterisation of samples having RCA-coils with immobilised probe-tagged beads

*2.3.2.1. Investigation of detection sensitivity (magnetisation spectrum vs. RCA-coil concentration).* 25 μl of the solution of probe-tagged beads was added to 25 μl of solution having different concentrations of RCA-products (0–300 pM after addition of probe-tagged beads) where the 0 pM sample was used as negative control sample. This mixture was gently homogenised at room temperature and 30 μl was extracted for immediate characterisation in the SQUID. The characterisation began with 30 min of incubation at 343 K (most optimal sample preparation procedure according to Strömberg et al., 2008), thereafter the complex magnetisation spectrum was measured at 310 K and finally the saturation magnetisation was determined at the same temperature. For clarity, the base-stacking calculated melting temperatures (BioMath) at the detection conditions (NaCl concentration 500 mM, $MgCl_2$ concentration 0 M and oligonucleotide concentration 10 nM) for the detection probes were all 336 K. However, since each bead has been functionalised with several oligonucleotides, the resulting melting temperature of the bead–RCA–product hybrids was larger than 336 K due to cooperative binding effects.

*2.3.2.2. Investigation of probe-tagged bead immobilisation kinetics.* The probe-tagged bead solution and the solution of RCA-coils were mixed as described above, but only one particular RCA-coil concentration was chosen. After extraction of 30 μl of the mixture, the HFP and LFP levels of $m''$ were recorded as a function of time (0–250 min) at constant temperature. The time decay of the $m''$ HFP level reflects the probe-tagged bead immobilisation kinetics.

## 3. Results and discussion

### 3.1. Comparing dynamical magnetic properties of non-functionalised and oligonucleotide probe-tagged beads of different sizes

Dynamical magnetic properties of bare and probe-tagged beads have been discussed in previous work (Strömberg et al., 2007a,b, 2008) and are here only reported in the supplementary material, section B.

### 3.2. Effects of varying the oligonucleotide surface coverage for 40 nm beads; "turn-on" and "turn-off" detection

Fig. 1 shows complex magnetisation spectra for samples with various RCA-coil concentrations, where batch I was used in (a) and (b) and batch II in (c) and (d). In both cases, target 1 and padlock probe 1 were used. The 0 pM curves (negative controls) correspond to samples free of RCA-products. Comparing panels (a) and (b) with panels (c) and (d) in Fig. 1, it can be observed that increasing the oligonucleotide surface coverage on the beads improves the bead immobilisation efficiency. This effect is explained by

**Table 1**
Synthesis conditions and properties of the oligonucleotide functionalised bead batches (upper half); sequences of padlock targets, padlock probes and detection probes (lower half)

| Original bead size (nm) | Batch no. | SPDP excess relative to total number of amine groups | Purification steps after SPDP addition | Oligonucleotide excess relative to number of beads | Oligonucleotide surface coverage | Purification steps after iodoacetamide addition | Batch dilution factor | Total batch dilution factor in final samples |
|---|---|---|---|---|---|---|---|---|
| 40[a] | I | 5.5 | 1 | 1,000 | 3 | 1 | 1 | 2 |
| 40[a] | II | 5.5 | 1 | 500 | 14 | 1 | 1 | 2 |
| 40[a] | III | 5.5 | 1 | 500 | 14 | 1 | 2 | 4 |
| 40[a] | IV | 5.5 | 1 | 500 | 6 | 1 | 1.5 | 3 |
| 40[a] | V | 5.5 | 1 | 500 | 6 | 1 | 2 | 4 |
| 130[a] | VI | 11 | 6 | 10,000 | 18 | 3 | 5 | 10 |
| 250[a] | VII | 11 | 6 | 61,350 | 54 | 3 | 4 | 8 |
| 250[a] | VIII | 11 | 6 | 30,725 | [e] | 3 | 10 | 20 |
| 250[c] | IX | 22 | 6 | 122,700 | [e] | 3 | – | – |
| 130[b] | X | 22 | 6 | 20,000 | [e] | 3 | – | – |
| 250[c] and 130[b] | XI[d] | – | – | – | – | – | 1 | 2 |

| Name | Sequence |
|---|---|
| Target 1 | 5′-GCAACAGTTCTTTATAATCCCGCTGTAATTAGCCCAGAAGAA-3′ |
| Padlock probe 1 | 5′-GGGATTATAAAGAACTGTTGCCTCGACCGTTAGCAGCATGATTCCGAGATGTACCGCTATCGTGTTGATGTCATGTGTCGCACTTCTTCTGGGCTAATTACAGC-3′ |
| Detection probe 1[f] | SH-5′-TTTTTTTTTTTTTTTTTTTTGTTGATGTCATGTGTCGCAC-3′-FITC |
| Target 2 | 5′-CCCTGGGCTCAACCTAGGAATCGCATTTG-3′ (*Vibrio cholerae* sequence) |
| Padlock probe 2 | 5′-TAGGTTGAGCCCAGGGACTTCTAGAGTGTACCGACCTCAGTAGCCGTGACTATCGACTTGTTGATGTCATGTGTCGCACCAAATGCGATTCC-3′ |
| Detection probe 2[f] | SH-5′-TTTTTTTTTTTTTTTTTTTTGTTGATGTCATGTGTCGCAC-3′-FITC |
| Target 3 | 5′-TTGTAAAGCACTTTCAGTTGTGAGGAAGGT-3′ (*Vibrio vulnificus* sequence) |
| Padlock probe 3 | 5′-ACTGAAAGTGCTTTACAACTTCTAGAGTGTACCGACCTCAGTAGCCGTGACTATCGACTCTGGACCTTAATCGTGTGCGACCTTCCTCACA-3′ |
| Detection probe 3 | SH-5′-TTTTTTTTTTTTTTTTTTTTCTGGACCTTAATCGTGTGCG-3′-FITC |

[a] Detection probe 1.
[b] Detection probe 3.
[c] Detection probe 2.
[d] IX and X mixed in volume amounts 1:3.
[e] Not analysed.
[f] Note that these probes are identical.

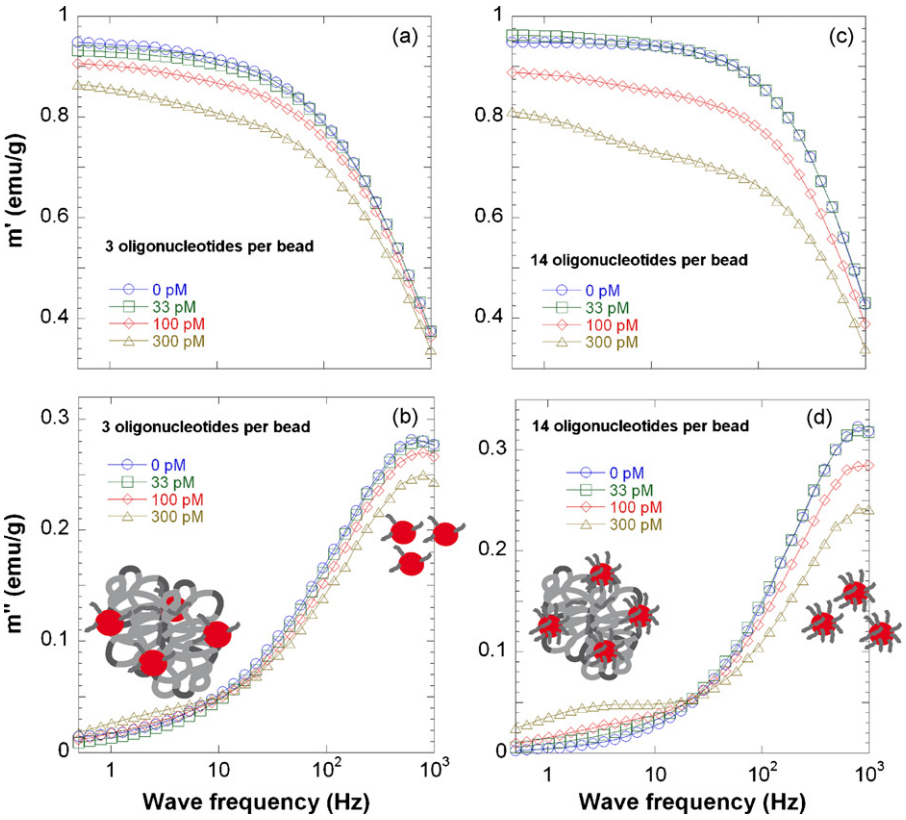


**Fig. 1.** Complex magnetisation vs. frequency at 310 K for 40 nm beads and RCA-coil concentrations ranging from 0 to 300 pM, where batch I was used in (a) and (b) and batch II in (c) and (d). In both cases, target 1 and padlock probe 1 were used. The upper and lower figure panels show the real and imaginary parts of the complex magnetisation, respectively. Probe-tagged beads and RCA-coils are illustrated by red solid spheres with dark-grey curved lines on surface and light-grey/black coils, respectively. Solid lines through data points are guides for the eye. (For interpretation of the references to color in this figure legend, the reader is referred to the web version of the article.)

the fact that a higher surface coverage of oligonucleotides yields more possibilities for a bead to hybridise to an RCA-coil. Another important observation is that, when using 40 nm beads, discrimination between positive and negative samples can be made using *both* the $m''$ HFP and LFP levels, which will be referred to as the "turn-off" and "turn-on" detection, respectively. The turn-off effect relates to the *decrease* in the $m''$ HFP level due to immobilisation of free beads in the RCA-coils, i.e. the number of free beads *decreases* in the solution medium. The turn-on effect relates to the *increase* in the $m''$ LFP level when the number of beads immobilised in coils *increases*. In our previous work using only 130 nm sized beads (Strömberg et al., 2008) discrimination between a negative and a positive sample could only be performed using turn-off detection. Using smaller beads opens up the possibility for discrimination in both the $m''$ HFP and LFP levels, and in some cases an improved discrimination in the $m''$ LFP levels is observed. To exemplify, the LOD in Fig. 1(b) is 100 pM in both the turn-off and the turn-on region, while the LOD in Fig. 1(d) is 33 pM in the turn-off and turn-on region, but with an improved discrimination between the various coil concentration curves in the turn-on region. The finding that both turn-on and turn-off detection is possible with small enough beads, whereas for large beads only turn-off detection is possible, give some indications of how beads with different sizes immobilise to RCA-coils. The possibility of turn-on detection is also attractive for future biosensor developments.

Due to the comparably low oligonucleotide coupling yield for the 40 nm beads, other surface coverages than for batches I and II were not investigated.

### 3.3. Effects of decreasing the concentration of 40 nm beads

Table S1 (supplementary material, section C) shows RCA-coil concentration, total number of RCA-coils and ratio between total number of beads and RCA-coils for the samples in Fig. 1(c) and (d), while Table S2 (supplementary material, section C) lists bead immobilisation characteristics for different bead sizes. One notices that the ratio between the total number of beads and RCA-coils is large, for instance it equals 442 for 33 pM RCA-coil concentration. This explains why a distinct discrimination cannot be made between the negative control sample and a positive sample with a very low RCA-coil concentration. In Fig. 1(c) and (d), for 14 oligonucleotides per bead, the LOD is 33 pM. On the other hand, in the 300 pM sample, around 11 beads are immobilised per coil, which is substantially more than for the 300 pM samples containing 130 and 250 nm beads, i.e. 3 and 0.14 immobilised beads per coil, respectively (cf. Table S2 in supplementary material, section C).

Fig. 2 shows the low frequency regions of the $m''$ spectra (0.5–20 Hz) for samples with various RCA-coil concentrations (target 1 and padlock probe 1); batches IV and III were used to obtain the results shown in panel (a) and (b), respectively. As can be observed, using a lower concentration of beads has a positive effect on the $m''$ LFP levels. There is an excellent correlation between the $m''$ LFP levels and the RCA-coil concentration, which was not observed previously (Strömberg et al., 2008). Lowering the bead concentration results in higher $m''$ LFP levels but also a larger spacing between the curves, i.e. the detection sensitivity is improved. This is expected since using a smaller amount of beads yields a higher percentage of immobilised beads for each coil concentration. However, there

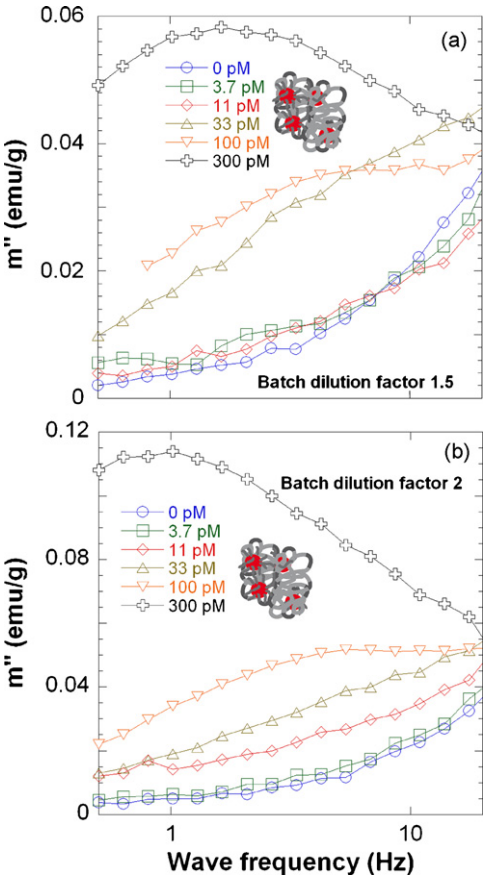


**Fig. 2.** The low-frequency regions of the imaginary part of complex magnetisation vs. frequency at 310 K for positive samples with 40 nm beads and RCA-coil concentrations ranging from 0 to 300 pM (target 1 and padlock probe 1 were used). Batches IV and III were used in (a) and (b), respectively. Probe-tagged beads and RCA-coils are illustrated by red solid spheres with dark-grey curved lines on surface and light-grey/black coils, respectively. Solid lines through data points are guides for the eye. Note the different $m''$ scales used in (a) and (b). (For interpretation of the references to color in this figure legend, the reader is referred to the web version of the article.)

is no significant improvement of the LOD comparing batches IV (Fig. 2(a)) and II (Fig. 1(d)). This is explained by the fact that the batch dilutions do not differ sufficiently much to induce a significant change of the LOD. The LOD in Fig. 2 is 33 pM in (a) and 11 pM in (b). Since the magnetic moment per bead is comparably small for the 40 nm beads, batch dilution by more than a factor 2 was not possible without yielding too poor signal to noise ratio.

### 3.4. Effects of varying the RCA-time for 40 nm beads

The effect of varying the RCA-time has been discussed in previous work (Strömberg et al., 2008) and the present results are therefore presented in the supplementary material, section D. As expected, increasing the RCA-time yields a higher degree of bead immobilisation. However, doubling the RCA-time from 60 to 120 min does not noticeably improve the immobilisation performance.

### 3.5. Effects of using large beads in low concentrations (250 nm beads)

Panels (a) and (b) in Fig. 3 show complex magnetisation spectra for samples with RCA-coil concentrations ranging from 0 to 300 pM (batch VII; target 1 and padlock probe 1 were used). The $m''$ profile for the 300 pM sample is featureless and small in magnitude, indicating that almost 100% of the beads are immobilised in the coils. The LOD for this concentration series is 11 pM, which is not as good as for the 130 nm beads investigated earlier (Strömberg et al., 2008), despite the fact that the concentration of beads is substantially smaller than in Strömberg et al. (2008). This observation is tentatively explained by the coil immobilisation capacity for larger beads being lower than for smaller beads due to sterical effects. Furthermore, no distinct low frequency peaks can be observed even for the highest RCA-coil concentrations despite the fact that the $m''$ HFP levels are so low. Beads are immobilised but in a different manner comparing with the immobilisation for the smaller sized beads. Most likely, small beads immobilise in the interior of the coils resulting in well separate coils with beads having a relaxation frequency around 1 Hz. The 250 nm beads on the other hand have a tendency to cross-link several coils, thus forming coil aggregates with relaxation frequencies below the low frequency limit of the ac magnetisation measurements (0.5 Hz). Another observation made for large beads is that immobilisation of 250 nm beads gives a much larger signal change than observed for the corresponding immobilisation of 40 nm beads.

Panels (c) and (d) in Fig. 3 show complex magnetisation spectra for positive samples with RCA-coil concentrations ranging from 0 to 300 pM (batch VIII; target 1 and padlock probe 1 were used). It can be seen that the $m''$ HFP levels have decreased (panel (d)) for all RCA-coil concentrations, the curve spacing has increased compared to that in Fig. 3(b) and the LOD is improved to 4 pM, which is the same limit as obtained for 130 nm beads (Strömberg et al., 2008). Moreover, in Fig. 3, it can be noticed that the HFPs are slightly shifted towards higher frequencies for increasing RCA-coil concentrations. A possible explanation for this is that the presence of RCA-coils decreases the number of free bead aggregates and/or the tendency for free beads to aggregate. The underlying physical mechanisms can be that the coils increase the separation between free beads by acting as physical barriers between the beads. In addition, coil hybridisation probability for aggregates of probe-tagged beads is most likely larger than for single beads due to a larger number of probe molecules per entity.

### 3.6. Immobilisation kinetics and immobilisation characteristics for different bead sizes

In a positive sample, i.e. when there is a match between the oligonucleotides on the bead surface and the sequence in the RCA-coils, the beads and coils approach each other through random diffusive motion and bind by hybridisation (Strömberg et al., 2008). When a bead is close enough to a coil hybridisation site, the hybridisation occurs instantaneously, i.e. the bead and coil diffusion is the rate determining step in the immobilisation process. In Strömberg et al. (2008), the kinetics was investigated only for 130 nm beads, and here immobilisation kinetics for two other bead sizes will be evaluated.

Fig. 4 shows the $m''$ HFP level vs. incubation time for three 100 pM positive samples (target 1 and padlock probe 1) with different bead sizes; 40 nm (batch V), 130 nm (batch I in Strömberg et al., 2008) and 250 nm (batch VII). The $m''$ HFP level is almost constant in time for the 40 and 130 nm beads and starts well below the corresponding negative control levels, which are around 0.35, 0.20 and 0.40 emu/g for the three sizes, respectively. This indicates that most of the 40 and 130 nm beads immobilise during the bead/coil mixing process and before the magnetic measurement begins, i.e. their immobilisation kinetics are very fast. This is expected because of their small size giving rise to large diffusion constants (Stokes–Einstein relation). However, the immobilisation kinetics for the 250 nm beads is unexpectedly slow compared to that of the 40 and 130 nm beads. The $m''$ HFP level starts slightly

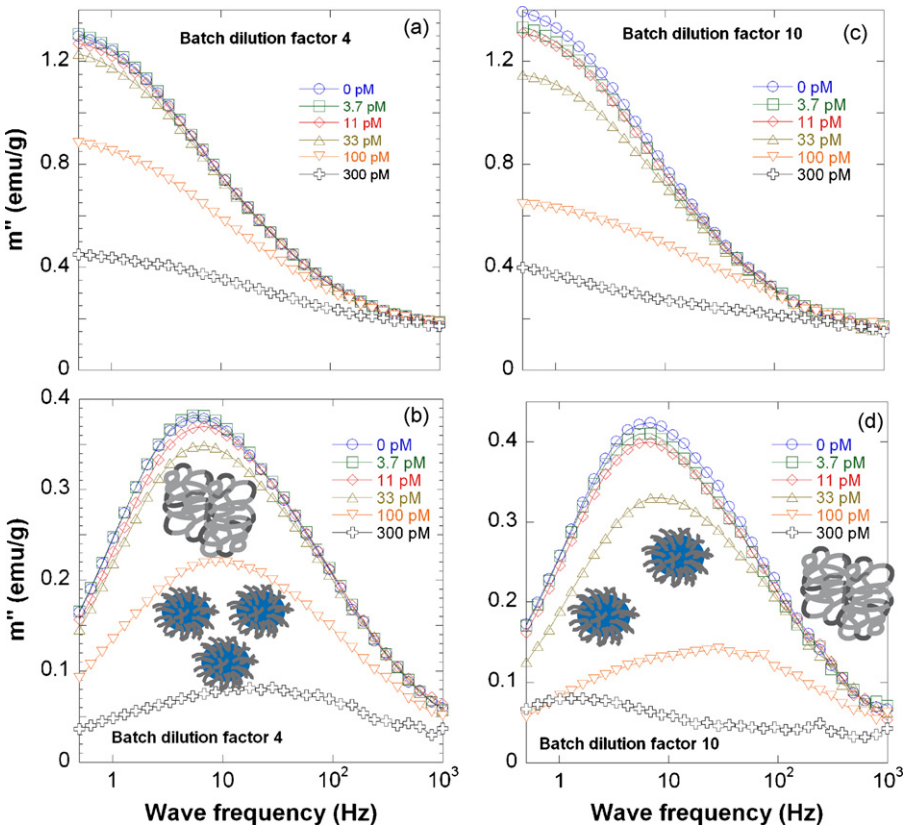


**Fig. 3.** Complex magnetisation vs. frequency at 310 K for samples with 250 nm beads and RCA-coil concentrations ranging from 0 to 300 pM, where batch VII was used in (a) and (b) and batch VIII in (c) and (d). In both cases, target 1 and padlock probe 1 were used. The upper and lower figure panels show the real and imaginary parts of the complex magnetisation, respectively. Probe-tagged beads and RCA-coils are illustrated by blue solid spheres with dark-grey curved lines on surface and light-grey/black coils, respectively. Solid lines through data points are guides for the eye. (For interpretation of the references to color in this figure legend, the reader is referred to the web version of the article.)

below the negative control level and decays slowly with time as it approaches the equilibrium $m''$ HFP level of the system. Most likely, as the results suggest, immobilisation kinetics is not only dependent on bead diffusion constant, which is directly related to bead size, but also on the fact that smaller beads due to steric reasons more easily find unoccupied hybridisation sites in the coils.

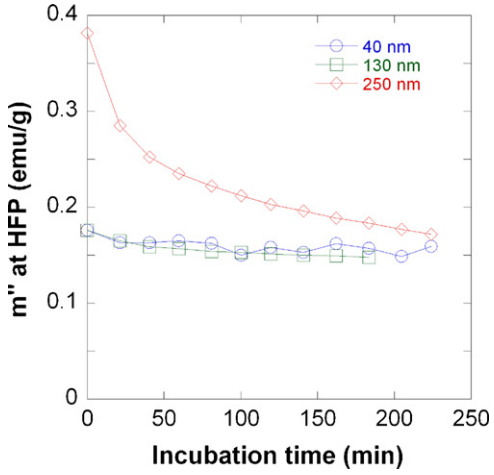


**Fig. 4.** High frequency peak level of the imaginary part of the complex magnetisation vs. incubation time at 310 K for three different samples containing a RCA-coil concentration of 100 pM (target 1 and padlock probe 1 were used) and beads of the displayed sizes; 40 nm (batch V), 130 nm (batch I in Strömberg et al., 2008) and 250 nm (batch VII). Solid lines through data points are guides for the eye.

Supplementary material, section C, provides a more detailed discussion of immobilisation characteristics for different bead sizes. Smaller beads exhibit faster immobilisation kinetics and occupy RCA-coils in larger amounts than larger beads. This makes small beads a better candidate for achieving a bioassay with improved characteristics.

### 3.7. Effects of reducing the concentration of 130 nm beads and adding a genomic background, sedimentation characteristics

In supplementary material, section E, the effects of reducing the concentration of 130 nm beads and adding genomic background material are discussed in detail (cf. Fig S3). The detection method is shown to work well even in presence of a large excess of background material added after ligation and RCA and the results even suggest a LOD approaching the 1 pM level. The results also indicate that the genomic background material decreases the bead sedimentation rate and/or bead adsorption tendency. Ligation and RCA have earlier been proven to perform robustly both in 0.05% pig feces and 12.5% whole blood (Jarvius et al., 2006).

### 3.8. Dual-target detection of biologically relevant targets (130 and 250 nm beads)

In this section, we qualitatively demonstrate for the first time simultaneous turn-off detection of two kinds of bacterial DNA sequences, *Vibrio cholerae* and *Vibrio vulnificus*, using a dual-size detection batch consisting of 250 and 130 nm beads. For obtaining

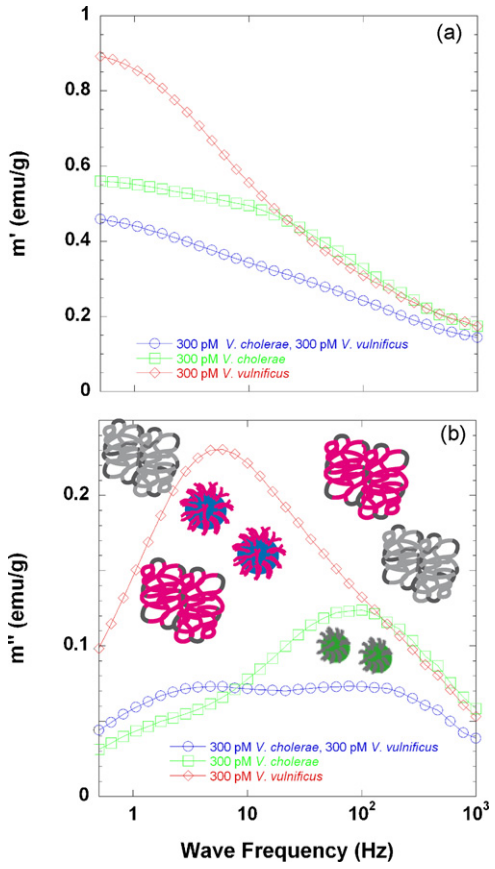


**Fig. 5.** Complex magnetisation vs. frequency at 310 K showing the results from a dual-target experiment involving *Vibrio cholerae* (250 nm beads, target 2 and padlock probe 2) and *Vibrio vulnificus* (130 nm beads, target 3 and padlock probe 3) DNA sequences (batch XI used). The curves indicated by blue circles, red squares and green squares show the responses for samples consisting of both *V. cholerae* and *V. vulnificus* targets, only *V. vulnificus* and only *V. cholerae* targets, respectively. In all samples, the probe-tagged bead concentration is 45 and 490 pM for 250 nm beads and 130 nm beads, respectively. Figure panels (a) and (b) show the real and imaginary parts of the complex magnetisation, respectively. RCA-coils arising from *V. Cholerae* and *V. Vulnificus* targets are illustrated as red/black and light-grey/black coils, respectively. Probe-tagged beads matching *V. Cholerae* and *V. Vulnificus* RCA-coils are illustrated as blue solid spheres with red curved lines on surface and green solid spheres with dark-grey curved lines on surface, respectively. Solid lines through data points are guides for the eye. (For interpretation of the references to color in this figure legend, the reader is referred to the web version of the article.)

the dual-size batch (XI), 250 and 130 nm beads (batches IX and X) were mixed in volume amounts 1:3.

Fig. 5 shows complex magnetisation spectra presenting the results from a dual-target experiment with *V. cholerae* (target 2 and padlock probe 2, 250 nm beads) and *V. vulnificus* (target 3 and padlock probe 3, 130 nm beads) DNA sequences. The real and imaginary parts of the complex magnetisation are shown in panels (a) and (b), respectively. In all samples, the probe-tagged bead concentration is 45 and 490 pM for 250 nm beads and 130 nm beads, respectively. We have here only characterised samples with high RCA-coil concentrations in order to qualitatively demonstrate that our bioassay allows for multiplexing. In a real situation, the RCA-coil concentrations may have all kinds of intermediate values. Furthermore, the results would have been easier to interpret if the free bead peak overlap was smaller, i.e. if the bead sizes differed more. Theoretically, in this case, quantitative analysis could be based on measuring the $m''$ HFP levels at the two free bead relaxation frequencies. However, this was not practically possible in this study due to the upper frequency limit of the used SQUID magnetometer being as low as 1 kHz. However, in the case of quantitative multiplexing, overlapping free bead peaks should not be a problem since the composite $m''$ signal can be deconvoluted in a similar manner as in Goldman et al. (2004), where multiplexed toxin analysis using four colours of quantum dot fluororeagents was performed. As can be seen in Fig. 5, the HFPs are located at 7 and 100 Hz for the 250 and 130 nm bead populations, respectively. If both targets are present, two relaxation peaks are detected. If only one of the targets is present, only one HFP can be observed, mainly arising from free beads having the opposite detection probe. In panel (a), it can be seen that the dual-target curve exhibits the smallest magnitude of the three curves, which is expected since this curve corresponds to the sample having the highest amount of immobilised beads.

Finally, a third relaxation process located around 1 Hz has to be taken into account to model the results of positive samples; the relaxation of the RCA-coils containing immobilised beads. Consequently, the measured magnetisation profile is a superposition of three peaks. However, when using beads of relatively large sizes as in this case, the height of the relaxation peak corresponding to RCA-coils containing immobilised beads is small enough not to significantly interfere with the 7 Hz peak corresponding to free probe-tagged 250 nm beads. This observation is consistent with the discussion in Section 3.6, where it was concluded that large beads form RCA-coil aggregates exhibiting a relaxation frequency outside the frequency range of the experiment.

## 4. Conclusion and outlooks

The effects of bead size, bead surface coverage of probe oligonucleotides, bead concentration and RCA-time on the performance of the volume amplified magnetic nanobead detection assay (Strömberg et al., 2008) have been evaluated, yielding several results of importance for future biosensor development. Summarising, the *three most fundamental and important results* are as follows: (i) using 40 nm beads, both *turn-off* and *turn-on* detection strategies are possible whereas only *turn-off* type detection is possible with larger beads. This observation is most likely an effect of differently sized beads immobilising to RCA-coils in different manners; large beads cross-link RCA-coils to form coil aggregates with characteristic frequencies outside the experimental frequency range. (ii) The *immobilisation kinetics* is faster for smaller beads and smaller beads immobilise in larger numbers to coils than larger beads. The faster immobilisation kinetics for small beads will be of importance for biosensor development, since the time needed to complete a diagnostic test is an essential parameter for the test performance. (iii) The bioassay can be used for *multiplexed detection*, which follows from the qualitative demonstration of dual-target detection of two kinds of bacterial DNA sequences using 130 and 250 nm beads.

Changing the read-out format by developing a miniaturised platform based on a magnetoresistive sensor (Freitas et al., 2007) or a micro-Hall probe (Sandhu et al., 2007; Mihajlovic et al., 2005), is expected to considerably improve the LOD. Moreover, by introducing a sensor that covers a broader frequency interval than that of the SQUID, a larger range of bead sizes can be implemented thus allowing for improved multiplexed detection strategies.

## Acknowledgements

The Knut and Alice Wallenberg Foundation (KAW), the Swedish Foundation for Strategic Research (SSF), the Swedish Defence Nanotechnology programme, and the Swedish Research Council (VR), are gratefully acknowledged for their financial support.

## Appendix A. Supplementary data

Supplementary data associated with this article can be found, in the online version, at doi:10.1016/j.bios.2008.06.043.

## References


Astalan, A.P., Ahrentorp, F., Johansson, C., Larsson, K., Krozer, A., 2004. Biosensors and Bioelectronics 19, 945–951.

BioMath—$T_m$ Calculations for Oligos, http://www.promega.com/biomath/calc11.htm.

Connolly, J., St Pierre, T.G., 2001. Journal of Magnetism and Magnetic Materials 225, 156–160.

Fire, A., Xu, S.-Q., 1995. Proceedings of the National Academy of Sciences of United States of America 92, 4641–4645.

Freitas, P.P., Ferreira, R., Cardoso, S., Cardoso, F., 2007. Journal of Physics: Condensed Matter 19, 165221.

Goldman, E.R., Clapp, A.R., Anderson, G.P., Uyeda, H.T., Mauro, J.M., Medintz, I.L., Mattoussi, H., 2004. Analytical Chemistry 76, 684–688.

Hong, C.-Y., Chen, W.S., Jian, Z.F., Yang, S.Y., Horng, H.E., Yang, L.C., Yang, H.C., 2007. Applied Physics Letters 90, 074105.

Jarvius, J., Melin, J., Göransson, J., Stenberg, J., Fredriksson, S., Gonzalez-Rey, C., Bertilsson, S., Nilsson, M., 2006. Nature Methods 3, 725–727.

Landegren, U., Dahl, F., Nilsson, M., Fredriksson, S., Banér, J., Gullberg, M., Jarvius, J., Gustafsdottir, S., Söderberg, O., Ericsson, O., Stenberg, J., Schallmeiner, E., 2003. Comparative and Functional Genomics 4, 525–530.

Liu, D., Daubendiek, S.L., Zillman, M.A., Ryan, K., Kool, E.T., 1996. Journal of the American Chemical Society 118, 1587–1594.

Liu, W.-T., 2006. Journal of Bioscience and Bioengineering 102, 1–7.

Majewski, P., Thierry, B., 2007. Critical Reviews in Solid State and Materials Sciences 32, 203–215.

Micromod Partikeltechnologie GmbH, http://www.micromod.de.

Mihajlovic, G., Xiong, P., von Molár, S., Ohtani, K., Ohno, H., Field, M., Sullivan, G.J., 2005. Applied Physics Letters 87, 112502.

Mornet, S., Vasseur, S., Grasset, F., Duguet, E., 2004. Journal of Materials Chemistry 14, 2161–2175.

Nilsson, M., Malmgren, H., Samiotaki, M., Kwiatkowski, M., Chowdhary, B.P., Landegren, U., 1994. Science 265, 2085–2088.

Osaka, T., Matsunaga, T., Nakanishi, T., Arakaki, A., Niwa, D., Iida, H., 2006. Analytical Bioanalytical Chemistry 384, 593–600.

Saiyed, Z.M., Telang, S.D., Ramchand, C.N., 2003. BioMagnetic Research and Technology 1, 2.

Salata, O.V., 2004. Journal of Nanobiotechnology 2, 3.

Sandhu, A., Kumagai, Y., Lapicki, A., Sakamoto, S., Abe, M., Handa, H., 2007. Biosensors and Bioelectronics 22, 2115–2120.

Strömberg, M., Gunnarsson, K., Valizadeh, S., Svedlindh, P., Strømme, M., 2007a. Journal of Applied Physics 101, 023911.

Strömberg, M., Gunnarsson, K., Johansson, H., Nilsson, M., Svedlindh, P., Strømme, M., 2007b. Journal of Physics D: Applied Physics 40, 1320–1330.

Strömberg, M., Göransson, J., Gunnarsson, K., Nilsson, M., Svedlindh, P., Strømme, M., 2008. Nano Letters 8, 816–821.

Wang, J., 2005. Small 1, 1036–1043.